Penerbit Akademia Baru

CFD Letters

Journal homepage: www.akademiabaru.com/cfdl.html
ISSN: 2180-1363

Study of Extracted Geometry Effect on Patient-Specific Cerebral Aneurysm Model with Different Threshold Coefficient (C_{thres})

Open Access

Lim Sheh Hong[1,*], Mohd Azrul Hisham Mohd Adib[1,*], Mohd Shafie Abdullah[2,3], Nur Hartini Mohd Taib[2,3], Radhiana Hassan[4], Azian Abd Aziz[4]

[1] Medical Engineering & Health Intervention Team (MedEHiT), Department of Mechanical Engineering, College of Engineering, Universiti Malaysia Pahang, 26600 Pekan, Pahang, Malaysia
[2] Department of Radiology, School of Medical Sciences, Health Campus, Universiti Sains Malaysia, 16150 Kubang Kerian, Kelantan, Malaysia
[3] Hospital Universiti Sains Malaysia, Health Campus, 16150 Kubang Kerian, Kelantan, Malaysia
[4] Department of Radiology, Kulliyyah of Medicine, International Islamic University Malaysia, 25200 Kuantan, Pahang, Malaysia

ARTICLE INFO

Article history:
Received 22 August 2020
Received in revised form 21 October 2020
Accepted 24 October 2020
Available online 30 October 2020

Keywords:
Cerebral aneurysm; threshold coefficient; hemodynamics; wall shear stress; computational fluid dynamics

ABSTRACT

The recent diagnostic assessment of cerebrovascular disease makes use of computational fluid dynamics (CFD) to quantify blood flow and determine the hemodynamics factors contributing to the disease from patient-specific models. However, compliant, and anatomical patient-specific geometries are generally reconstructed from the medical images with different threshold values subjectively. Therefore, this paper tends to present the effect of extracted geometry with different threshold coefficient, C_{thres} by using a patient-specific cerebral aneurysm model. A set of medical images, digital subtraction angiography (DSA) images from the real patient diagnosed with internal carotid artery (ICA) aneurysm was obtained. The threshold value used to extract the patient-specific cerebral aneurysm geometry was calculated by using a simple threshold determination method. Several threshold coefficients, C_{thres} such as 0.2, 0.3, 0.4, 0.5 and 0.6 were employed in the image segmentation creating three-dimensional (3D) realistic arterial geometries that were then used for CFD simulation. As a result, we obtained that the volume of each patient-specific cerebral aneurysm geometry decreases as the threshold coefficient, C_{thres} increases. There is dislocation of artery attached to the ICA aneurysm geometry occurred at a high threshold coefficient, C_{thres}. Besides, the physical changes also bring remarkable physiological effect on the wall shear stress (WSS) distribution and velocity flow field at the patient-specific cerebral aneurysm geometry reconstructed with different threshold coefficient, C_{thres}.

[*] *Corresponding author.*
E-mail address: shehhong.lim@gmail.com (Lim Sheh Hong)
E-mail address: azrul@ump.edu.my (Mohd Azrul Hisham Mohd Adib)

https://doi.org/10.37934/cfdl.12.10.114

1. Introduction

The evolution and implementation of medical imaging in the diagnosis of cerebrovascular diseases have provided an abundance of information in terms of physiological and pathological conditions on particular cerebrovascular system [1]. Besides, the analysis of hemodynamics in the cerebrovascular system can be acquired more accurately and specifically through computational study on the anatomical geometry. The establishment to combine computational fluid dynamics (CFD) on anatomical geometry with medical imaging of arterial geometry has become the current trend which makes the studies of hemodynamics and vascular diseases to a higher extent closer to the actual condition extracted in vivo which may not be performed as always [2-4]. This alternatively allows estimation of numerous hemodynamics parameters such as wall shear stress (WSS), location of impact zone, impingement at the arterial wall and blood residence indicating the initiation and progression of vascular pathologies [2, 5-7].

However, some studies have claimed that the outputs such as WSS and velocity vector from the image-based CFD simulations are varied with the actual phantom and the most possible cause is the acquired in vivo geometry from the medical images [2]. Besides, some researchers have conducted experiments by applying particle image velocimetry (PIV) and validated their results with the CFD phantoms, they came out with the same consensus that the variations or slight changes in geometries contribute to aneurysmal flow significantly by 50–60% [8-11]. The variations in the acquired CFD geometry have been claimed influencing the hemodynamics and physiological behavior of blood flow along the vascular structure creating local shear stress, unidirectional flow and flow circulation [12-14] other than the temporal and spatial boundary conditions which are implemented in the CFD simulation [15-16].

Although the extraction and conversion of anatomical model geometry from the medical images to CFD geometries can be done manually or automatically but subjectively with the available software packages [10, 17], it is crucial to obtain the anatomically realistic geometry as the analysis of hemodynamics strongly depends on the model configuration [18-19]. In order to obtain the anatomically realistic geometry, image segmentation is performed by extracting the object of interest from the medical images, however the geometry might not be reconstructed consistently if it is extracted by trial and error [6, 20-21]. Therefore, in the present study, the image segmentation was performed systematically by adjusting the threshold image intensity calculated through threshold determination method introduced by Omodaka *et al.,* [22] and CFD simulation was performed on the anatomical cerebral aneurysm geometries to identify the consistency of location among the geometries created with different threshold coefficient, C_{thres}.

2. Methodology

2.1 Determination of Threshold Image Intensity

The present investigation uses 768 slices of digital subtraction angiography (DSA) images obtained from a 48 years old male patient diagnosed with internal carotid artery (ICA) aneurysm in the year of 2012. The imaging was performed on an Allura Xper FD20 angiography system (Philips Medical Systems B.V., The Netherlands) with rotational angiography program at International Islamic University Malaysia Medical Centre (IIUM-MC), Kuantan, Pahang. The acquired rotational frames were directed to an independent workstation (XtraVision, Philips Healthcare, The Netherlands). The two-dimensional (2D) images in DICOM based were exported to *ImageJ* and presented in 8-bit with 256 x 256 acquisition matrices to extract the image intensity for threshold determination through Eq. (1).

$$I_{thres} = C_{thres}(I_{max} - I_{min}) + I_{min} \tag{1}$$

where I_{thres} refers to the threshold image intensity, C_{thres} refers to the threshold coefficient, while I_{min} and I_{max} refer to the minimum and maximum values of the image intensity along the line probe, respectively. A line probe was constructed at the representative cross-section of the proximal artery as shown in Figure 1 to measure the image intensity. A profile curve of the image intensity was generated according to the line probe across the artery as shown in Figure 2.

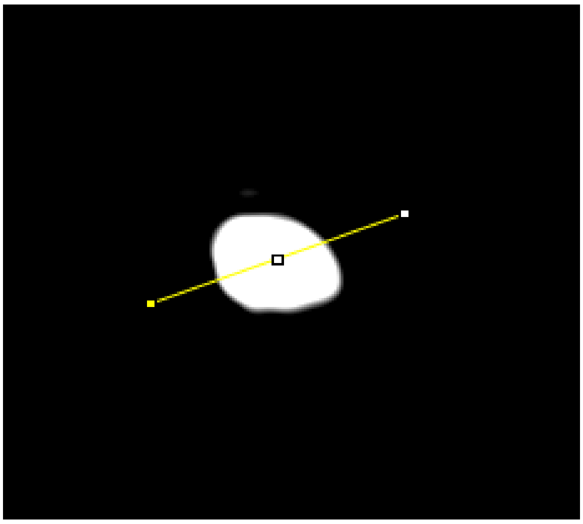

Fig. 1. Line probe at representative cross-section of proximal artery

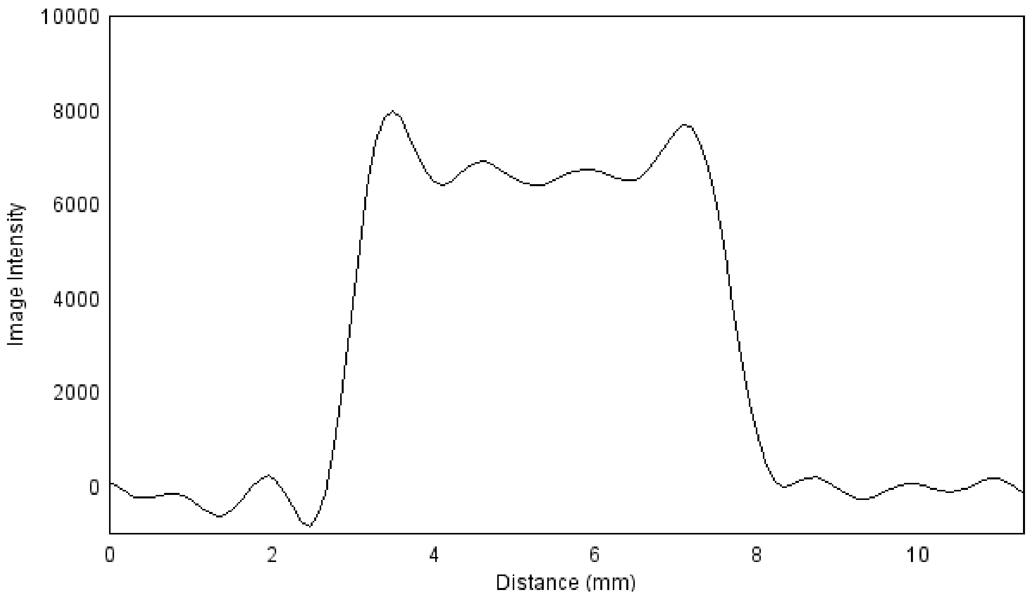

Fig. 2. Profile curve along the line probe

In the present data, the image intensity ranges between 7.56 and 7997.27. The minimum and maximum values of the image intensity along the line probe, I_{min} and I_{max} were obtained. They were then used to determine the threshold image intensity, I_{thres} with different threshold coefficient, C_{thres} such as 0.2, 0.3, 0.4, 0.5 and 0.6 by using the formula defined in Eq. (1). The calculated values of threshold image intensity, I_{thres} as listed in Table 1 were then used for image segmentation in *AMIRA^{TM} 2019.3*.

Table 1
Values of threshold image intensity with respective threshold coefficient

Threshold coefficient, C_{thres}	Threshold image intensity, I_{thres}
0.2	1605.501
0.3	2404.473
0.4	3203.444
0.5	4002.415
0.6	4801.386

2.2 Governing Equation of Blood Flow

The blood flow in artery is considered to be incompressible and the governing equations applied for computational domain, Ώ are Navier-Stokes and continuity equations as follows:

$$\frac{\partial u_i}{\partial x_i} = 0 \tag{2}$$

$$\rho\left(\frac{\partial u_i}{\partial t} + u_j \frac{\partial u_i}{\partial x_i}\right) = -\frac{\partial P}{\partial x_j} + \mu \frac{\partial^2 u_i}{\partial x_j \partial x_j} + f_i \tag{3}$$

where u_i refers to the velocity in the i^{th} direction, P refers to the pressure, f_i refers to the body force, ρ refers to the density, μ refers to the viscosity and ∂_{ij} refers to the Kronecker delta.

The shear stress, τ at the aneurysm wall is calculated through the function of velocity gradient as follows:

$$\tau = \mu \frac{\partial u}{\partial y} \tag{4}$$

where $\frac{\partial u}{\partial y}$ refers to the velocity gradient along the aneurysm wall with regard to the fluid viscosity. Therefore, the simple viscous fluid is considered as linear relationship. The equation of motion in terms of vorticity, ω is defined as follows:

$$\frac{\partial \omega}{\partial t} - \nabla \times (u \times \omega) = \frac{\mu}{\rho} \nabla^2 \omega \tag{5}$$

where ω refers to the vorticity, ρ refers to the density and μ refers to the viscosity with vector $\nabla^2 u$ evaluated. These equations are accomplished and solved in finite volume form through CFD solver, *ANSYS Fluent 16.2*.

2.3 Boundary Condition

The aneurysm wall is considered to be no-slip condition throughout this investigation as follows:

$$u = 0 \tag{6}$$

The fluid, blood is considered as incompressible, laminar, Newtonian fluid with isothermal constant viscosity of 0.0035 Pa.s [23]. The blood density is 1060 kg/m^3 [24] with reference to the average normal human blood density. The temperature, specific heat and thermal conductivity of blood are set as 310 K, 3513 J/kg.K and 0.44 W/m.K [25], respectively. As the present investigation concerns on the effect of extracted geometry with different threshold coefficient, the inlet velocity is fixed at 0.3 m/s [26], which is also the average peak systolic velocity [27] obtained from the previous studies for consistency. The boundary condition was only defined at the inlet and there was no constraint defined at the outlets for the present simulation. The parameters used for boundary condition set up are listed in Table 2.

Table 2
Parameters used for boundary condition set up

Parameters	Value
Viscosity (Pa.s)	0.0035
Density (kg/m^3)	1060
Temperature (K)	310
Specific heat (J/kg.K)	3513
Thermal conductivity (W/m.K)	0.44
Inlet velocity (m/s)	0.3

3. Results and Discussion
3.1 Extracted Geometry with Different Threshold Coefficient

Five three-dimensional (3D) geometries have been extracted, segmented and reconstructed with respective threshold coefficient, C_{thres} as listed in Table 1. The 3D geometries are shown in Figure 3 while the geometry with the indication of inlet and outlets is illustrated in Figure 4. The geometry reconstructed with $C_{thres} = 0.6$ is excluded from the computational study as its geometry does not comply with and is beyond the actual shape among the others.

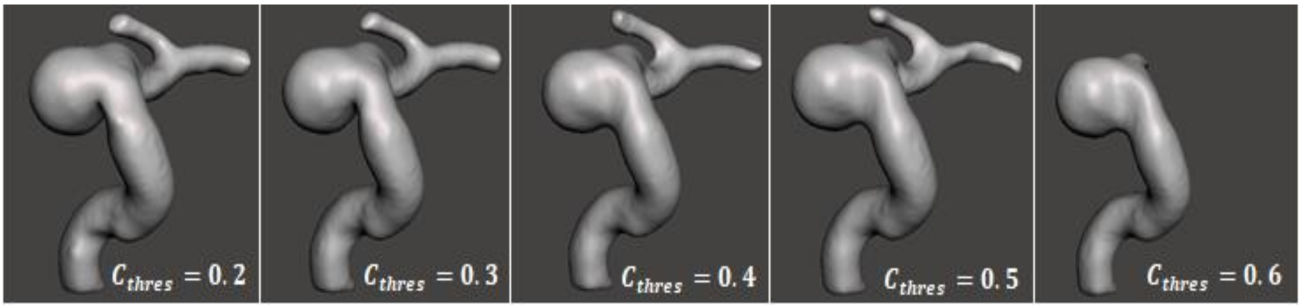

Fig. 3. 3D geometries with respective threshold coefficient, C_{thres}

By comparing among the geometries, there is no significant change in term of shape except for the geometry reconstructed with C_{thres} of 0.6. There is disconnection and disappearance of the branch where bifurcation exists. Furthermore, it can be noticed that the arteries after bifurcation become narrower as the C_{thres} increases. This might be due to the vasculature adherence to the object of interest which leads to the physical change, the volume of the patient-specific cerebral aneurysm geometries with arteries reduces as the C_{thres} increases and thus, causing some important parts to be marked out unconsciously. Indeed, the volume reduction is found to have correspondence with the inlet and outlet areas as listed in Table 3 with regard to respective geometry reconstructed with C_{thres} of 0.2, 0.3, 0.4 and 0.5. Besides, the volume reduction is within 10% of difference with each other when C_{thres} increases as illustrated in Figure 5.

According to the previous research, it was reported that geometry configuration has high impact on the aneurysmal hemodynamics [28]. Some researchers also claim that small arteries can be neglected for physiological analysis as compared to the large arteries which have high visualization

[6]. However, further investigation was conducted regarding the effect of extracted geometry by taking all arteries (inlet and outlet) into account which is discussed in the following section.

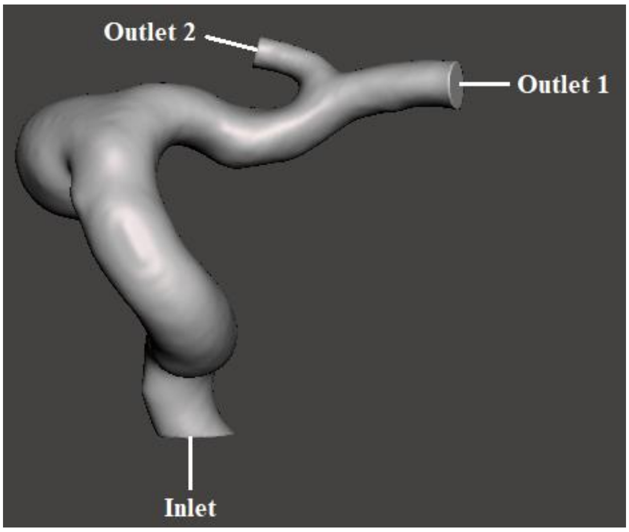

Fig. 4. Geometry with indication of inlet and outlets

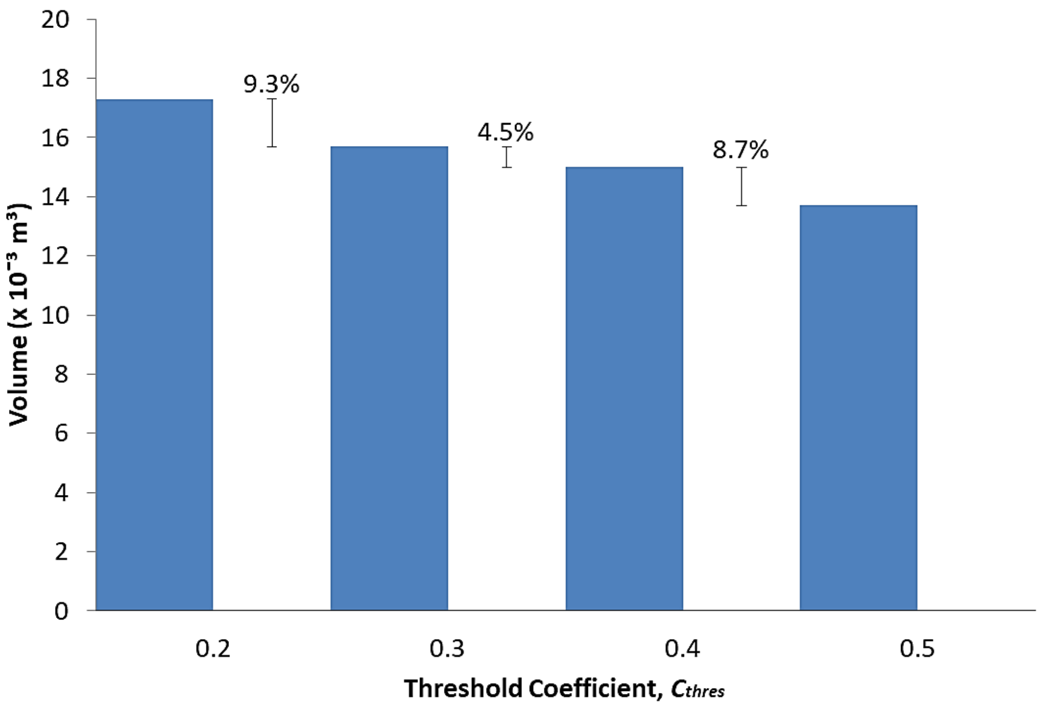

Fig. 5. Representation of geometry volume with percentage difference

Table 3
Volume, inlet and outlet areas extracted from respective geometry

Geometries	Volume (m^3)	Inlet area (m^2)	Outlet 1 area (m^2)	Outlet 2 area (m^2)
0.2	17.3×10^{-3}	13.6×10^{-3}	4.35×10^{-3}	2.31×10^{-3}
0.3	15.7×10^{-3}	11.8×10^{-3}	3.52×10^{-3}	1.90×10^{-3}
0.4	15.0×10^{-3}	11.0×10^{-3}	2.63×10^{-3}	1.84×10^{-3}
0.5	13.7×10^{-3}	10.6×10^{-3}	1.50×10^{-3}	1.33×10^{-3}

3.2 Wall Shear Stress (WSS) Distribution

Based on the in vitro simulation on the anatomical geometries reconstructed from the patient-specific cerebral aneurysm model, the visualization of WSS distribution in the direction of *x-z* projection is obtained as shown in Figure 6. Some studies have reported that 45% of the maximum WSS has been found at the neck of the aneurysm, followed by 40% at the bifurcation, 10% at the aneurysm dome and 5% at the parent artery [29-31]. The assessment on the geometries at present investigation has found that the WSS was cultivated at the neck of aneurysm and artery where bifurcation exists. This has the same correlation with the previous studies. Also, the WSS was concentrated at the outlet 2 with small area which can be seen clearly at the geometries reconstructed with C_{thres} of 0.4 and 0.5. However, the WSS distribution at the aneurysm region at each of the geometry is relatively low. Table 4 shows the maximum WSS of respective geometry reconstructed with C_{thres} of 0.2, 0.3, 0.4 and 0.5. The magnitude of maximum WSS increases after C_{thres} of 0.2.

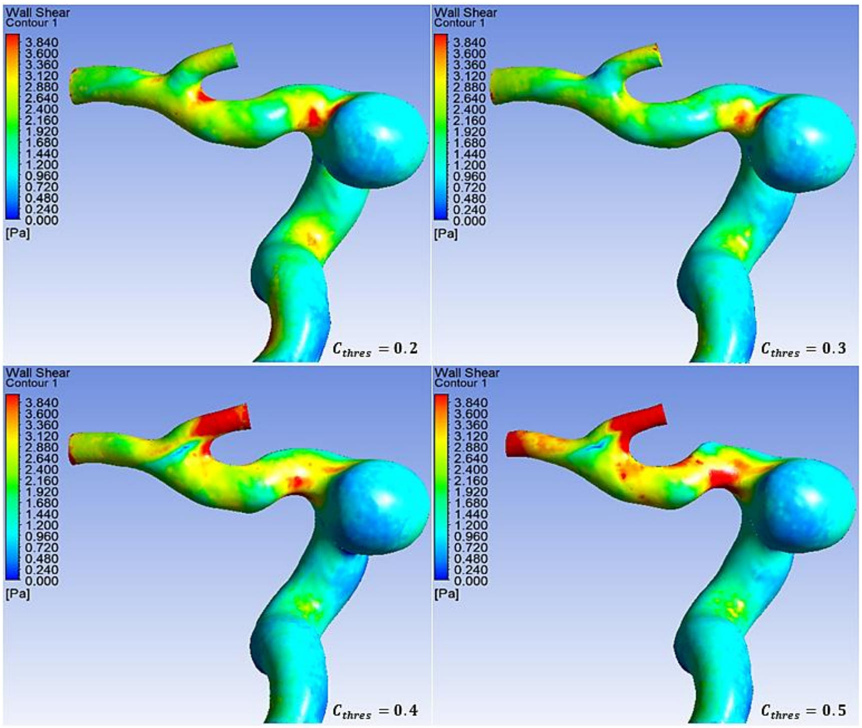

Fig. 6. Representation of WSS distribution with respective threshold coefficient, C_{thres}

Generally, the WSS is directly proportional to the velocity component as defined in Eq. (4) in theoretical framework [32]. In the present case, the blood passed through the aneurysm has come to the meet point and merged to the outlets after the bifurcation part with high velocity due to the vortex or circulation flow in the aneurysm. Therefore, the WSS is seen to be highly concentrated at the narrower outlet 2 as compared to outlet 1. The location of WSS distribution from the simulation results is considered consistent. However, the location of WSS distribution might be varied with the previous studies due to the assumptions used for simulating blood flow [33] and replication of aneurysm geometry which does not compromise the realistic aneurysm geometries [34]. Hence, the mesh quality and simulation result are affected. Furthermore, the shape of aneurysm geometries strongly depends on the reconstruction technique especially through medical images and this technically affects the WSS distribution and hemodynamics at the aneurysm geometries [26, 35].

Table 4
Maximum WSS extracted from respective geometry

Geometries	Maximum WSS (Pa)
0.2	8.00
0.3	6.43
0.4	14.84
0.5	32.89

3.3 Velocity Flow Field

The velocity vector and streamline flow are illustrated in Figure 7 and Figure 8, respectively. The velocity flow fields in the anatomical aneurysm geometries are highly complex as expected. From the initial location (inlet) where the blood flew towards the aneurysm region, the blood velocity maintained at around 0.2 – 0.3 m/s. After the blood exited right after the aneurysm region towards the bifurcation part, the blood velocity increased promptly towards the outlets. There is flow impingement intensified only after the aneurysm but not in the aneurysm region [4]. The blood velocity has achieved almost five times than the assumed inlet velocity. This might be probably due to the vortex or circulation flow which improves the blood velocity [36-38]. Also, the blood has merged to two outlets, causing the blood velocity to be extreme at the arteries where bifurcation exists. This would increase the aneurysm initiation and rupturing possibility as well as the atherosclerotic plaques formation to be occurred at the mentioned locations. Table 5 shows the maximum velocity of respective geometry reconstructed with C_{thres} of 0.2, 0.3, 0.4 and 0.5. The magnitude of maximum velocity increases after C_{thres} of 0.2, which has the same trend as the magnitude of WSS distribution as discussed in the previous section. However, there is only one helical circulation present in the aneurysm region at each of the geometry which has contradiction with the previous studies [39-41].

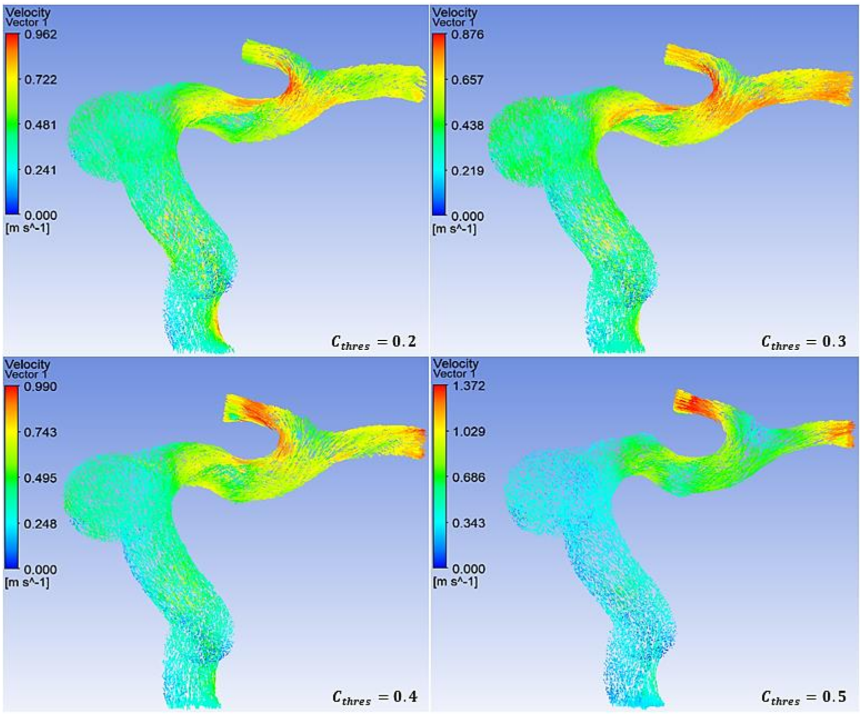

Fig. 7. Representation of velocity vector with respective threshold coefficient, C_{thres}

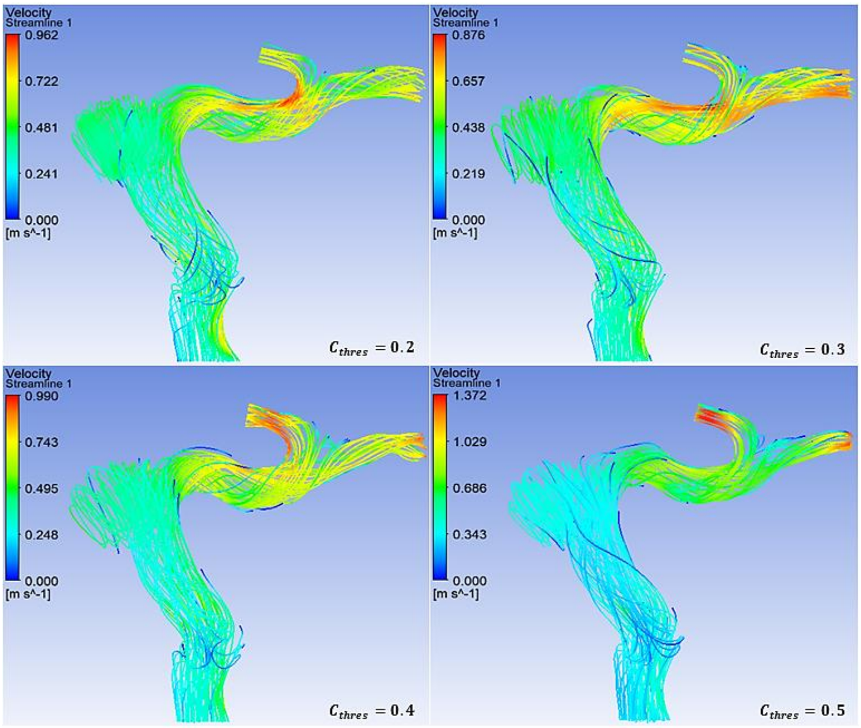

Fig. 8. Representation of velocity streamline with respective threshold coefficient, C_{thres}

Table 5
Maximum velocity extracted from respective geometry

Geometries	Maximum velocity (m/s)
0.2	0.98
0.3	0.86
0.4	0.95
0.5	1.36

3.4 Mesh Independence and Validation

In order to make sure the result obtained from the computational simulation is precise and trustworthy, it is required to perform mesh independence test on the object of interest with different mesh size to determine the suitable mesh which best represents the behavior of the geometry prior to results analysis. In the present investigation, several simulations had been performed on the geometry reconstructed with C_{thres} of 0.2 by defining several mesh, from coarse mesh to fine mesh ranging from 0.1 – 0.01m.

According to the generated results as indicated in Figure 9, Figure 10 and Table 6, the critical parameters such as maximum WSS and velocity have slight variations. However, the volume, inlet and outlet areas have no change, indicating the meshing done was well adapted to the reconstructed geometry. Although the result variations of maximum WSS and velocity are not significant, it can still be observed that the results were circulating along the dotted line as shown in Figure 9 and Figure 10, respectively. The mesh size of 0.05m is chosen to apply on the rest of the reconstructed geometries in the current investigation for consistency as this mesh size is able to give better results with less computational cost as compared to finer mesh. Therefore, the simulation results as discussed in this investigation are based on the reconstructed geometries with mesh size of 0.05m.

CFD Letters
Volume 12, Issue 10 (2020) 1-14

Since the results from the simulation are incapable to be validated through experimental studies due to uncertainties on the physiological and pathological aspects [2], it has been reported that the WSS distribution and velocity flow field are sensitive to the local geometry [15, 17, 42]. Besides, CFD simulation is not able to validate in vivo hemodynamics accurately and precisely [3, 11, 43]. Therefore, the simulation results would be used to compare with magnetic resonance imaging (MRI) image, which is acquired through magnetic and radio waves in future framework for further analysis and validation.

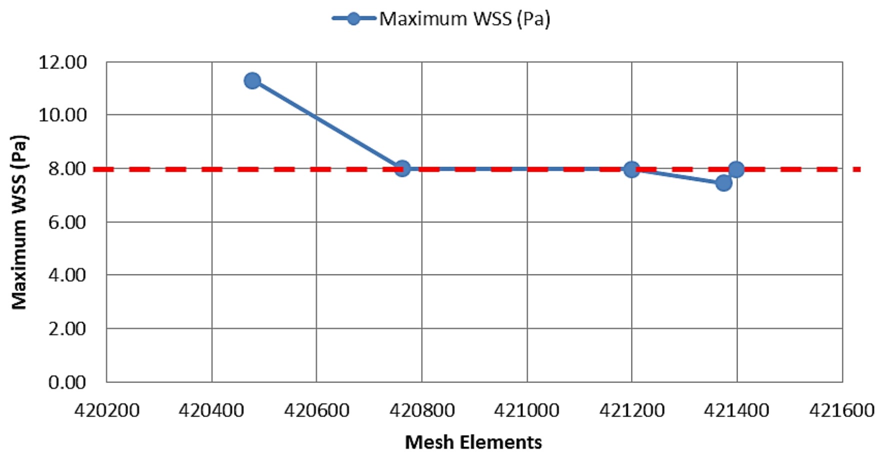

Fig. 9. Graph of maximum WSS against mesh elements for geometry reconstructed with threshold coefficient, C_{thres} of 0.2

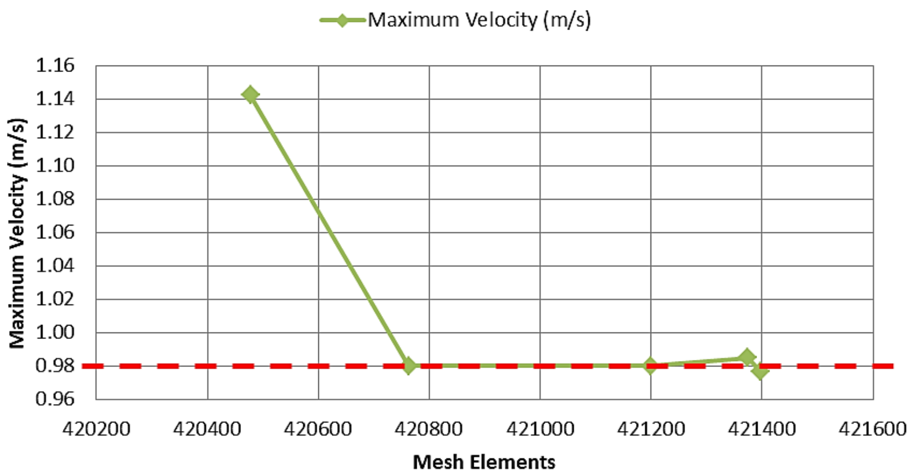

Fig. 10. Graph of maximum velocity against mesh elements for geometry reconstructed with threshold coefficient, C_{thres} of 0.2

Table 6
Details of applied mesh size with physical output from geometry reconstructed with threshold coefficient, C_{thres} of 0.2

Mesh size (m)	Mesh element	Maximum WSS (Pa)	Maximum velocity (m/s)
0.10	420478	11.30	1.14
0.05	420763	8.00	0.98
0.03	421199	7.97	0.98
0.02	421375	7.45	0.98
0.01	421398	7.98	0.97

4. Conclusion

The simulation results from the present investigation show that the reconstruction of anatomical aneurysm geometry has strong influence on the analysis of hemodynamics, especially on minute and complex geometry which makes the analytical work to be exhausted. The reconstruction of aneurysm geometry through image segmentation with different threshold coefficient, C_{thres} from medical image has shown significant physical changes on the aneurysm geometry in terms of shape, volume, inlet and outlet areas. Indeed, the hemodynamics which has high sensitivity to the geometry is affected as well. The WSS distribution and velocity flow field are among the crucial parameters to predict the initiation and rupturing of aneurysm. Although the results have slight variation with the previous studies, there is enough evidence showing that the locations where the aneurysm initiation and rupturing as well as atherosclerotic plaques formation are most probably to be occurred. The locations with significant WSS distribution and velocity flow field have good correspondence among the other geometries. Besides, the accurate estimation on the magnitude of WSS distribution and velocity flow field would be achieved in conjunction with in vivo measurements from MRI image in future framework.

Acknowledgement

The support from Universiti Malaysia Pahang under grant RDU190153, Ministry of Higher Education (MOHE) under FRGS grant (FRGS/1/2018/TK03/UMP/02/23) and MedEHiT are gratefully acknowledged.

References

[1] MacDonald, Matthew Ethan, and Richard Frayne. "Cerebrovascular MRI: a review of state-of-the-art approaches, methods and techniques." *NMR in Biomedicine* 28, no. 7 (2015): 767-791. https://doi.org/10.1002/nbm.3322

[2] Hoi, Yiemeng, Scott H. Woodward, Minsuok Kim, Dale B. Taulbee, and Hui Meng. "Validation of CFD simulations of cerebral aneurysms with implication of geometric variations." (2006): 844-851. https://doi.org/10.1115/1.2354209

[3] Moore, J. A., DAs Steinman, D. W. Holdsworth, and C. R. Ethier. "Accuracy of computational hemodynamics in complex arterial geometries reconstructed from magnetic resonance imaging." *Annals of biomedical engineering* 27, no. 1 (1999): 32-41. https://doi.org/10.1114/1.163

[4] Hoi, Yiemeng, Hui Meng, Scott H. Woodward, Bernard R. Bendok, Ricardo A. Hanel, Lee R. Guterman, and L. Nelson Hopkins. "Effects of arterial geometry on aneurysm growth: three-dimensional computational fluid dynamics study." *Journal of neurosurgery* 101, no. 4 (2004): 676-681. https://doi.org/10.3171/jns.2004.101.4.0676

[5] Cebral, Juan R., Peter J. Yim, Rainald Löhner, Orlando Soto, and Peter L. Choyke. "Blood flow modeling in carotid arteries with computational fluid dynamics and MR imaging." *Academic radiology* 9, no. 11 (2002): 1286-1299. https://doi.org/10.1016/S1076-6332(03)80562-7

[6] Cebral, Juan R., Marcelo Adrián Castro, Sunil Appanaboyina, Christopher M. Putman, Daniel Millan, and Alejandro F. Frangi. "Efficient pipeline for image-based patient-specific analysis of cerebral aneurysm hemodynamics: technique and sensitivity." *IEEE transactions on medical imaging* 24, no. 4 (2005): 457-467. https://doi.org/10.1109/TMI.2005.844159

[7] Jou, Liang-Der, Christopher M. Quick, William L. Young, Michael T. Lawton, Randall Higashida, Alastair Martin, and David Saloner. "Computational approach to quantifying hemodynamic forces in giant cerebral aneurysms." *American Journal of Neuroradiology* 24, no. 9 (2003): 1804-1810. https://pubmed.ncbi.nlm.nih.gov/14561606

[8] Lieber, Baruch B., Veronica Livescu, L. N. Hopkins, and Ajay K. Wakhloo. "Particle image velocimetry assessment of stent design influence on intra-aneurysmal flow." *Annals of biomedical engineering* 30, no. 6 (2002): 768-777. https://doi.org/10.1114/1.1495867

[9] Liou, Tong-Miin, and Shuenn-Nan Liou. "A review on in vitro studies of hemodynamic characteristics in terminal

and lateral aneurysm models." *Proceedings of the National Science Council, Republic of China. Part B, Life sciences* 23, no. 4 (1999): 133.
https://pubmed.ncbi.nlm.nih.gov/10518314

[10] Ernemann, Ulrike U., Eckart Grönewäller, Frank B. Duffner, Oezlem Guervit, Joerg Claassen, and Martin D. Skalej. "Influence of Geometric and Hemodynamic Parameters on Aneurysm Visualization during Three-Dimensional Rotational Angiography: An in Vitro Study." *American Journal of Neuroradiology* 24, no. 4 (2003): 597–603.
https://pubmed.ncbi.nlm.nih.gov/12695187/

[11] Moore, Jennifer A, David A Steinman, and C Ross Ethier. "Computational Blood Flow Modelling: Errors Associated with Reconstructing Finite Element Models from Magnetic Resonance Images." *Journal of Biomechanics* 31, no. 2 (1997): 179–84.
https://doi.org/10.1016/S0021-9290(97)00125-5

[12] Ku, D. N., D. P. Giddens, D. J. Phillips, and D. E. Strandness Jr. "Hemodynamics of the normal human carotid bifurcation: in vitro and in vivo studies." *Ultrasound in medicine & biology* 11, no. 1 (1985): 13-26.
https://doi.org/10.1016/0301-5629(85)90003-1

[13] Zarins, Christopher K, Don P Giddens, B K Bharadvaj, Vikrom S Sottiurai, Robert F Mabon, and Seymour Glagov. "Carotid Bifurcation Atherosclerosis. Quantitative Correlation of Plaque Localization with Flow Velocity Profiles and Wall Shear Stress." *Circulation Research* 53, no. 4 (1983): 502–514.
https://doi.org/10.1161/01.RES.53.4.502

[14] Sawchuk, Alan P., Joseph L. Unthank, Thomas E. Davis, and Michael C. Dalsing. "A prospective, in vivo study of the relationship between blood flow hemodynamics and atherosclerosis in a hyperlipidemic swine model." *Journal of vascular surgery* 19, no. 1 (1994): 58-64.
https://doi.org/10.1016/s0741-5214(94)70120-2

[15] Augst, A. D., D. C. Barratt, A. D. Hughes, F. P. Glor, S. A. Thom, and X. Y. Xu. "Accuracy and reproducibility of CFD predicted wall shear stress using 3D ultrasound images." *Journal of biomechanical engineering* 125, no. 2 (2003): 218-222.
https://doi.org/10.1115/1.1553973

[16] Oshima, Marie, Hiroyuki Sakai, and Ryo Torii. "Modelling of inflow boundary conditions for image-based simulation of cerebrovascular flow." *International journal for numerical methods in fluids* 47, no. 6-7 (2005): 603-617.
https://doi.org/10.1002/fld.834

[17] Thomas, Jonathan B., Jaques S. Milner, Brian K. Rutt, and David A. Steinman. "Reproducibility of image-based computational fluid dynamics models of the human carotid bifurcation." *Annals of biomedical engineering* 31, no. 2 (2003): 132-141.
https://doi.org/10.1114/1.1540102

[18] Tadjfar, Mehran. "Flow into an arterial branch model." *Journal of engineering mathematics* 54, no. 4 (2006): 359-374.
https://doi.org/10.1007/s10665-006-9031-8

[19] Cebral, Juan Raul, and Rainald Löhner. "From medical images to anatomically accurate finite element grids." *International Journal for Numerical Methods in Engineering* 51, no. 8 (2001): 985-1008.
https://doi.org/10.1002/nme.205

[20] Chang, Herng-Hua, Gary R. Duckwiler, Daniel J. Valentino, and Woei Chyn Chu. "Computer-assisted extraction of intracranial aneurysms on 3D rotational angiograms for computational fluid dynamics modeling." *Medical physics* 36, no. 12 (2009): 5612-5621.
https://doi.org/10.1118/1.3260841

[21] Rayz, Vitaliy L., Loic Boussel, Gabriel Acevedo-Bolton, Alastair J. Martin, William L. Young, Michael T. Lawton, Randall Higashida, and David Saloner. "Numerical simulations of flow in cerebral aneurysms: comparison of CFD results and in vivo MRI measurements." *Journal of biomechanical engineering* 130, no. 5 (2008).
https://doi.org/10.1115/1.2970056

[22] Omodaka, Shunsuke, Takashi Inoue, Kenichi Funamoto, Shin-ichirou Sugiyama, Hiroaki Shimizu, Toshiyuki Hayase, Akira Takahashi, and Teiji Tominaga. "Influence of surface model extraction parameter on computational fluid dynamics modeling of cerebral aneurysms." *Journal of biomechanics* 45, no. 14 (2012): 2355-2361.
https://doi.org/10.1016/j.jbiomech.2012.07.006

[23] Adib, Mohd Azrul Hisham Mohd, Satoshi Ii, Yoshiyuki Watanabe, and Shigeo Wada. "Minimizing the blood velocity differences between phase-contrast magnetic resonance imaging and computational fluid dynamics simulation in cerebral arteries and aneurysms." *Medical & biological engineering & computing* 55, no. 9 (2017): 1605-1619.
https://doi.org/10.1007/s11517-017-1617-y

[24] Rispoli, Vinicius C., Jon F. Nielsen, Krishna S. Nayak, and Joao LA Carvalho. "Computational fluid dynamics simulations of blood flow regularized by 3D phase contrast MRI." *Biomedical engineering online* 14, no. 1 (2015):

110.
https://doi.org/10.1186/s12938-015-0104-7
[25] Akshaya, B, G Atchaya, Barakath Nisha A, K Hemalatha, T Tamilarasan, and M Shanmugavalli. "Blood Flow Analysis in Thoracic Aorta During Aneurysm." *International Journal of Innovative Research in Electrical, Electronics, Instrumentation and Control Engineering* 8, no. 3 (2020): 40–44.
https://doi.org/10.17148/IJIREEICE.2020.8307
[26] Hong, Lim Sheh, Mohd Azrul Hisham Mohd Adib, Mohd Shafie Abdullah, and Radhiana Hassan. "Qualitative and Quantitative Comparison of Hemodynamics Between MRI Measurement and CFD Simulation on Patient-specific Cerebral Aneurysm–A Review." *Journal of Advanced Research in Fluid Mechanics and Thermal Sciences* 68, no. 2 (2020): 112-123.
https://doi.org/10.37934/arfmts.68.2.112123
[27] Samijo, Steven K., Jean M. Willigers, Peter J. Brands, Richard Barkhuysen, Robert S. Reneman, Peter JEHM Kitslaar, and Arnold PG Hoeks. "Reproducibility of shear rate and shear stress assessment by means of ultrasound in the common carotid artery of young human males and females." *Ultrasound in medicine & biology* 23, no. 4 (1997): 583-590.
https://doi.org/10.1016/s0301-5629(97)00044-6
[28] Mohd Adib, Mohd Azrul Hisham, and Nur Hazreen Mohd Hasni. "Effect on the reconstruction of blood vessel geometry to the thresholds image intensity level for patient aneurysm." In *Journal of Biomimetics, Biomaterials and Biomedical Engineering*, vol. 22, pp. 89-95. Trans Tech Publications Ltd, 2015.
https://doi.org/10.4028/www.scientific.net/JBBBE.22.89
[29] Adib, Mohd, and Mohd Azrul Hisham. "Measurement of threshold image intensities on difference of vascular model: Effect on computational fluid dynamics for patient-specific cerebral aneurysm." In *Journal of Biomimetics, Biomaterials and Biomedical Engineering*, vol. 27, pp. 55-59. Trans Tech Publications Ltd, 2016.
https://doi.org/10.4028/www.scientific.net/JBBBE.27.55
[30] Chen, Jia-liang, Guang-hong Ding, Xin-jian Yang, and Hai-yun Li. "Effects of Parent Artery Segmentation and Aneurismalwall Elasticity on Patient-Specific Hemodynamic Simulations." *Journal of Hydrodynamics* 23, no. 5 (2011): 660-668.
https://doi.org/10.1016/S1001-6058(10)60162-X
[31] Kroon, Martin. "Simulation of Cerebral Aneurysm Growth and Prediction of Evolving Rupture Risk." *Modelling & Simulation in Engineering* 2011 (2011).
https://doi.org/10.1155/2011/289523
[32] Stainier, Laurent. "A variational approach to modeling coupled thermo-mechanical nonlinear dissipative behaviors." In *Advances in Applied Mechanics*, vol. 46, pp. 69-126. Elsevier, 2013.
https://doi.org/10.1016/B978-0-12-396522-6.00002-5
[33] Mahrous, Samar A., Nor Azwadi Che Sidik, and M. Saqr Khalid. "Newtonian and non-Newtonian CFD Models of Intracranial Aneurysm: A Review." *CFD Letters* 12, no. 1 (2020): 62-86.
[34] Schubiger, O., A. Valavanis, and W. Wichmann. "Growth-mechanism of giant intracranial aneurysms; demonstration by CT and MR imaging." *Neuroradiology* 29, no. 3 (1987): 266-271.
https://doi.org/10.1007/BF00451765
[35] Taylor, Charles A., and David A. Steinman. "Image-based modeling of blood flow and vessel wall dynamics: applications, methods and future directions." *Annals of biomedical engineering* 38, no. 3 (2010): 1188-1203.
https://doi.org/10.1007/s10439-010-9901-0
[36] Lugt, Hans J. "Vortex Flow in Nature and Technology.Fig" New York, Wiley-Interscience, 1983, 305 p. Translation., 1983.
https://doi.org/10.1115/1.3167650
[37] Pozniak, Myron A., and Paul L. Allan. *Clinical Doppler Ultrasound E-Book: Expert Consult: Online*. Elsevier Health Sciences, 2013.
https://books.google.com.my/books?id=SYCzAQAAQBAJ.
[38] Howarth, Charles B, John J De Marco, and John R Shanebrook. "Vortex Blood Pump BT - Heart Replacement." edited by Tetsuzo Akutsu and Hitoshi Koyanagi, 74–78. Tokyo: Springer Japan, 1998.
https://doi.org/10.1007/978-4-431-65921-1_11
[39] Botnar, R., M. B. Scheidegger, and P. Boesiger. "Quantification of blood flow patterns in human vessels by magnetic resonance imaging." *Technology and Health Care* 4, no. 1 (1996): 97-112.
https://doi.org/10.3233/THC-1996-4111
[40] Botnar, René, Gerhard Rappitsch, Markus Beat Scheidegger, Dieter Liepsch, Karl Perktold, and Peter Boesiger. "Hemodynamics in the carotid artery bifurcation:: a comparison between numerical simulations and in vitro MRI measurements." *Journal of biomechanics* 33, no. 2 (2000): 137-144.

https://doi.org/10.1016/S0021-9290(99)00164-5

[41] Rayz, V. L., L. Boussel, M. T. Lawton, G. Acevedo-Bolton, L. Ge, W. L. Young, R. T. Higashida, and D. Saloner. "Numerical modeling of the flow in intracranial aneurysms: prediction of regions prone to thrombus formation." *Annals of biomedical engineering* 36, no. 11 (2008): 1793. https://doi.org/10.1007/s10439-008-9561-5

[42] Katz, I M, E J Shaughnessy, and B B Cress. "A Technical Problem in the Calculation of Laminar Flow near Irregular Surfaces Described by Sampled Geometric Data." *Journal of Biomechanics* 28, no. 4 (1995): 461–64. https://doi.org/10.1016/0021-9290(94)00086-J

[43] Milner, Jaques S., Jennifer A. Moore, Brian K. Rutt, and David A. Steinman. "Hemodynamics of human carotid artery bifurcations: computational studies with models reconstructed from magnetic resonance imaging of normal subjects." *Journal of vascular surgery* 28, no. 1 (1998): 143-156. https://doi.org/10.1016/S0741-5214(98)70210-1